set (Fig. 3B), and we extracted a Bell state fidelity of 0.72, which demonstrates the production of an entangled state. For $\tau = \tau_{ent} = \frac{\pi}{(2J_{12})} = 160$ ns (Fig. 3C), we see a similar state to $\tau = 140$ ns, but with less weight in the single-qubit components of the Pauli set. This state corresponds to the intended CPhase of π, although the fidelity is slightly lower than at $\tau = 140$ ns due to additional decoherence. Finally, at $\tau = \pi/J_{12} = 320$ ns (Fig. 3D), where we expect the state to be unentangled, we again see large weight in the $\langle YI \rangle$, $\langle IY \rangle$, and $\langle YY \rangle$

emission (*23*), we calculated the lifetime for quantum dots (QDs) placed in the near field of this metamaterial. Our simulation takes into account nonidealities arising because of realistic losses, dispersion, finite thickness of layers, sample size, and the substrate. Even in a practical structure (Fig. 2B), a clear modification in lifetime of the emitter is expected as the system transitions from elliptical to the hyperbolic dispersion regime over the spectral range of interest. The transition occurs because of the particular dispersion of coupled plasmons, which contribute to lifetime decrease only on the hyperbolic side of the transition (*21*). Simulations carried out through effective medium theory (EMT) show good agreement with the prediction of numerical simulations (Fig. 2B).

To experimentally observe the signature of the predicted OTT manifested through enhancement in spontaneous emission rate, we investigated a metamaterial structure similar to that discussed above with multiple QD emitters positioned on its top surface (Fig. 3A) (*21*). The dielectric constants of the constituent thin films were extracted by using ellipsometry, and the effective medium parameters are shown in Fig. 3B. This structure is designed to have $\varepsilon_{\parallel} \approx 0$ around 621 nm, which corresponds to the emission maximum of the CdSe/ZnS colloidal QDs used in the experiment. The photoluminescence (PL) from the QDs has a full width at half maximum (FWHM) of ~40 nm, which allows investigation of the phase space of both elliptical and hyperbolic dispersion regimes by use of the same sample. In order to isolate the effects of the nonradiative decay and SPP-based enhancement in the radiative rate due to the metal, we also measured the spontaneous emission rates of QDs on a control sample that consisted of one unit cell of the metamaterial (*21*).

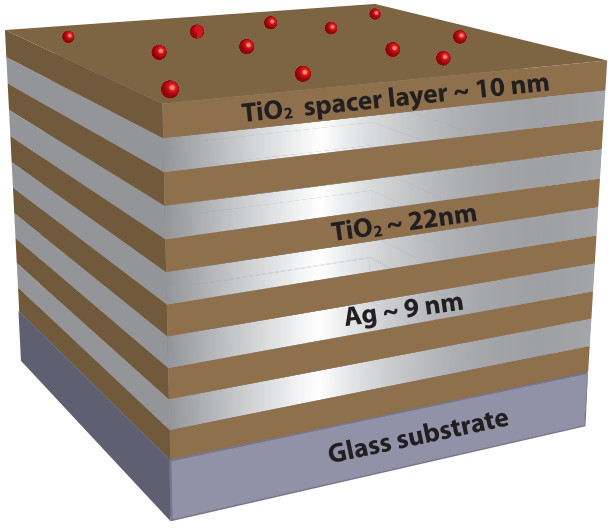

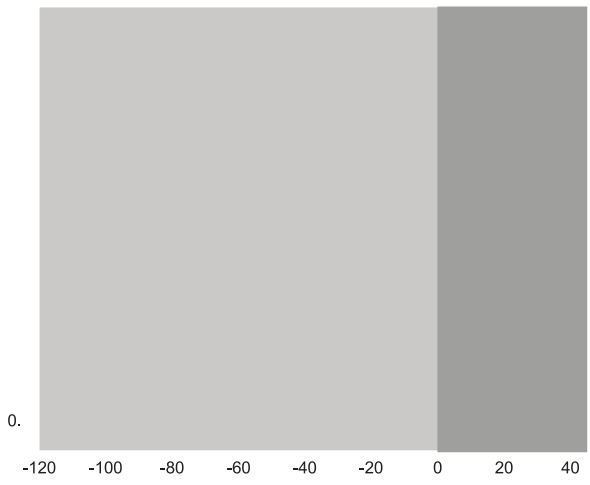

Fig. 4. The lifetime on the metamaterial structures normalized with respect to the control samples. The wavelength axis has been normalized with respect to the transition wavelength to compare the three samples. Here, positive and negative $\Delta\lambda$ correspond to hyperbolic and elliptical dispersion regimes, respectively. The samples with fill fractions of 29 and 33% show the OTT manifested through sharp reduction in spontaneous emission lifetime when crossing over to the hyperbolic dispersion regime. On the contrary, the sample with 23% fill fraction, which lies in the elliptical dispersion regime, does not show such a reduction in lifetime. The experimentally observed transition is in good agreement with the theoretical prediction of Fig. 2B.

Time-resolved PL measurements were carried out on the metamaterial sample, the control sample, and the glass substrate (Fig. 3C) at the anticipated transition wavelength (621nm) and at spectral positions on either side (605 and 635 nm). The large change in the spontaneous emission lifetime of the QDs on the metamaterial compared with the glass substrate is due to the excitation of the high-k metamaterial states as well as the nonradiative contribution and the SPP modes of the metamaterial. When compared with the control sample, the metamaterial shows an enhancement in the spontaneous emission rate by a factor of ~3 at the transition wavelength and ~4.3 deeper in the hyperbolic regime (635 nm). These enhancements are attributed to the high-k metamaterial states. The overall reduction in the lifetime of the QDs when compared with those on a glass substrate is ~11.

The lifetime of the QDs increases as a function of wavelength on both the glass substrate and the control sample (Fig. 3D). This is due to the size distribution of QDs and the dependence of the oscillator strength on the energy (*24*–*26*). On the contrary, the metamaterial sample shows a decrease in the lifetime as a function of wavelength and the shortest lifetime owing to coupling to the high-k metamaterial states (Fig. 3D). The coupling of the emission from the QDs into the metamaterial states was also verified by using steady-state PL measurements (fig. S6) in which a reduction in the PL intensity emitted in the direction away from the metamaterial sample was observed (*21*, *27*).

To demonstrate the OTT, we studied the radiative lifetimes in three samples with differing volume ratio of metal to dielectric, which correspond to different transition wavelengths. We compared the lifetimes of the sample with 29% fill fraction of silver to one with 23% fill fraction, which lies deep in the elliptical phase, and to another sample that lies deeper in the hyperbolic phase, with fill fraction of 33% (*21*). To make any conclusions regarding the effect of the OTT on the radiative lifetimes from the measurement of the total decay rates, the contribution of the high-k metamaterial states has to be distinguished from nonradiative decay and the SPP-assisted decay of the unit cell. Because the spacer and first-layer environment of the QDs is the same in the control and the metamaterial sample, we expected similar quantum yield dependence on wavelength owing to near-field interaction of the QDs and the metallic structure. Thus, to account for purely the contribution from the high-k metamaterial states to the overall lifetime change, we normalized the QD lifetime on the metamaterials with that on the control samples (Fig. 4). The controls for the three samples are different and correspond to the unit cell of each metamaterial sample. To compare these three samples, which have OTTs at different wavelengths, we normalized the wavelength with respect to the transition wavelength, with positive and negative $\Delta\lambda$ corresponding to the hyperbolic and elliptical dispersion regimes, respectively.

We clearly observed a sharp reduction in the normalized lifetime of the samples with 29 and 33% fill fractions that cross the transition wavelength, whereas the sample with 23% fill fraction, which lies in the elliptical regime, did not show this reduction. Whereas the combination of metal losses and finite thickness of layers leads to a smooth crossover, the signature of the transition is clear from the reduction in the normalized lifetime in the hyperbolic regime. The difference in the absolute value of the normalized lifetimes in the two samples that show the transitions is due to the differing fill fractions (29 versus 33%) and associated difference in the dielectric constants. Thus, the changes in the lifetime observed experimentally in these metamaterial structures can be attributed to the increase in the photonic density of states that manifests when the system goes through the topological transition in its isofrequency surface from an ellipsoid to a hyperboloid, which is in good agreement with the theoretical prediction of Fig. 2B.

We have established the occurrence of OTT in two metamaterial structures using spontaneous emission from a quantum emitter as the probe. Absence of OTT in a structure that lies solely in the elliptical dispersion phase has also been demonstrated. A host of interesting effects can transpire at the transition wavelength, such as the sudden appearance of resonance cones, which are characteristic of hyperbolic metamaterials (*28*), enhanced nonlinear effects, and abrupt changes in the electromagnetic energy density. We expect the OTT to be the basis for a number of applications of both fundamental and technological importance through use of metamaterial-based control of light-matter interaction.

References and Notes

1. V. M. Shalaev, *Nat. Photonics* **1**, 41 (2007).
2. J. B. Pendry, *Phys. Rev. Lett.* **85**, 3966 (2000).
3. J. B. Pendry, D. Schurig, D. R. Smith, *Science* **312**, 1780 (2006).
4. U. Leonhardt, *Science* **312**, 1777 (2006).
5. D. A. Genov, S. Zhang, X. Zhang, *Nat. Phys.* **5**, 687 (2009).
6. E. E. Narimanov, A. V. Kildishev, *Appl. Phys. Lett.* **95**, 041106 (2009).
7. I. I. Smolyaninov, E. E. Narimanov, *Phys. Rev. Lett.* **105**, 067402 (2010).
8. Z. Jacob, L. V. Alekseyev, E. Narimanov, *Opt. Express* **14**, 8247 (2006).
9. Z. Liu, H. Lee, Y. Xiong, C. Sun, X. Zhang, *Science* **315**, 1686 (2007).
10. M. Nakahara, *Geometry, Topology and Physics* (IOP Publishing, Bristol, UK, ed. 2, 2003).
11. M. Monastryskiy, *Riemann Topology and Physics* (Birkhäuser, Boston, ed.2, 1999).
12. I. M. Lifshitz, *Sov. Phys. JETP* **11**, 1130 (1960).
13. A. M. Kosevich, *Low Temp. Phys.* **30**, 97 (2004).
14. M. Born, E. Wolf, *Principles of Optics* (Cambridge Univ. Press, Cambridge, ed. 7, 2002).
15. P. Yao *et al.*, *Phys. Rev. B* **80**, 195106 (2009).
16. Z. Jacob, I. Smolyaninov, E. Narimanov, arXiv:0910.3981v2 [physics.optics] (2009).
17. M. A. Noginov *et al.*, *Opt. Lett.* **35**, 1863 (2010).
18. Z. Jacob *et al.*, *Appl. Phys. B* **100**, 215 (2010).
19. A. N. Poddubny, P. A. Belov, Y. S. Kivshar, *Phys. Rev. A* **84**, 023807 (2011).
20. O. Kidwai, S. V. Zhukovsky, J. E. Sipe, *Opt. Lett.* **36**, 2530 (2011).
21. A complete description of the fabrication, characterization, and modeling is available as supplementary materials on *Science* Online.
22. A. J. Hoffman *et al.*, *Nat. Mater.* **6**, 946 (2007).
23. G. W. Ford, W. H. Weber, *Phys. Rep.* **113**, 195 (1984).
24. M. D. Leistikow, J. Johansen, A. J. Kettelarij, P. Lodahl, W. L. Vos, *Phys. Rev. B* **79**, 045301 (2009).
25. M. L. Andersen, S. Stobbe, A. S. Sørensen, P. Lodahl, *Nat. Phys.* **7**, 215 (2011).
26. K. Okamoto, S. Vyawahare, A. Scherer, *J. Opt. Soc. Am. B* **23**, 1674 (2006).
27. I. Contijo *et al.*, *Phys. Rev. B* **60**, 11564 (1999).
28. L. B. Felsen, N. Marcuvitz, *Radiation and Scattering of Waves* (IEEE, New York, 1994).

Acknowledgments: V.M.M. and H.N.S.K. acknowledge partial support through the Materials Research Science and Engineering Center program of the National Science Foundation through grant DMR 1120923 and the Army Research Office (ARO) grant W911NF0710397. V.M.M. and I.K. acknowledge support through Round 14 of the CUNY Collaborative Incentive Research Grant Program. E.N. was partially supported by ARO–Multidisciplinary University Research Initiative grants 50342-PH-MUR and W911NF-09-1-0539. Z.J. was partially

supported by Natural Sciences and Engineering Research Council of CanadaDiscovery grant 402792 and Canadian School of Energy and Environment Proof of Principle Grant. The ellipsometric measurements were carried out at the Center for Functional Nanomaterials at Brookhaven National Laboratory, which is supported by the U.S. Department of Energy, Office of Basic Energy Sciences, under contract DE-AC02-98CH10886.

Supplementary Materials

www.sciencemag.org/cgi/content/full/336/6078/205/DC1
Materials and Methods
Figs. S1 to S6
References (*29*, *30*)

16 January 2012; accepted 7 March 2012
10.1126/science.1219171

Ferroelectric Columnar Liquid Crystal Featuring Confined Polar Groups Within Core–Shell Architecture

Daigo Miyajima,[1] Fumito Araoka,[2] Hideo Takezoe,[2]* Jungeun Kim,[3] Kenichi Kato,[4] Masaki Takata,[3,4] Takuzo Aida[1]*

Ferroelectric liquid crystals are materials that have a remnant and electrically invertible polar order. Columnar liquid crystals with a ferroelectric nature have potential use in ultrahigh-density memory devices, if electrical polarization occurs along the columnar axis. However, columnar liquid crystals having an axial nonzero polarization at zero electric field and its electrical invertibility have not been demonstrated. Here, we report a ferroelectric response for a columnar liquid crystal adopting a core–shell architecture that accommodates an array of polar cyano groups confined by a hydrogen-bonded amide network with an optimal strength. Under an applied electric field, both columns and core cyano groups align unidirectionally, thereby developing an extremely large macroscopic remnant polarization.

Ferroelectric liquid crystals (FLCs) have potential application in lightweight, easy-processable electrical devices for fast-switching displays, rewritable memories, and nonlinear optics (*1*). For liquid crystalline (LC) materials to operate ferroelectrically, a nonzero polarization at zero electric field (E-field), together with its electrical invertibility, is a prerequisite. However, this goal is difficult to realize, particularly in dynamic molecular systems such as LC materials, as once oriented electrically, polar motifs reorganize spontaneously at zero E-field in such a way that their dipoles cancel each other either macroscopically or locally. Although FLCs with a smectic geometry (Fig. 1, A and)

Topological Transitions in Metamaterials

Harish N. S. Krishnamoorthy, Zubin Jacob, Evgenii Narimanov, Ilona Kretzschmar and Vinod M. Menon

Science **336** (6078), 205-209.
DOI: 10.1126/science.1219171

Manipulating Optical Topology

Phase transitions in solid-state systems are often associated with a drastic change in the properties of that system. For example, metal-to-insulator transition or magnetic-to-nonmagnetic states find wide application in memory storage technology. An exotic electronic phase transition is the Lifshitz transition, whereby the Fermi surface undergoes a change in topology and a drastic change in the electronic density of states. **Krishnamoorthy *et al.*** (p. 205) now show that the notion of such a phase transition can be carried over to the optical regime by the suitable design of a metamaterial structure. This effect could be used to control the interaction between light and matter.